Supplementary Information for the manuscript entitled:
Impacts of ocean albedo alteration on Arctic sea ice recovery and global climate

Ivana Cvijanovic*
Carnegie Institution for Science, Department of Global Ecology, Stanford, California, USA; Now at: Atmospheric, Earth and Energy Division, Lawrence Livermore National Laboratory, Livermore, California, USA
ivanacv@llnl.gov

Ken Caldeira
Carnegie Institution for Science, Department of Global Ecology, Stanford, California, USA
kcaldeira@carnegiescience.edu

and

Douglas G. MacMartin
California Institute of Technology, Department of Computing + Mathematical Sciences, Pasadena, California, USA
macmardg@cds.caltech.edu

a) High latitude surface energy budget decomposition

Over the area 60° to 90°N, imposed albedo modifications in alb70-90N relative to $4xCO_2$ simulation lead to a surface albedo increase of 0.115 ± 0.022 (Supplementary Table 2) and upwelling (reflected) surface shortwave radiation increase of 0.44 ± 0.01 PW (~41 %) (Supplementary Table 5). Since in the $4xCO_2$ simulation 2.84 ± 0.01 PW of downward shortwave radiation reaches the surface, with everything else unchanged this would lead to an increase of 0.33 PW (=0.115×2.84) in reflected shortwave radiation in alb70-90N relative to $4xCO_2$. However, due to an additional increase in shortwave downward radiation at the surface of 0.22 ± 0.01 PW, upward shortwave radiation at the surface actually increases by 0.44 ± 0.01 PW (0.44 PW= 0.375×0.22 PW + 0.115×2.84 PW + 0.115×0.22 PW; where 0.375 is a surface albedo in the $4xCO_2$ simulation, Supplementary Table 2). Increase in shortwave downward radiation at the surface in alb70-90N relative to the 4xCO2 simulation is predominantly a consequence of a decreased cloud cover: corresponding clear-sky shortwave downward radiation increase is only 0.04 PW.

Net shortwave radiation from the surface over the area 60° to 90°N (difference between the upward and downward shortwave flux) increases by 0.21±0.01 PW in alb70-90 relative to the $4xCO_2$ simulation.

---

* Corresponding Author

As a consequence of increased ice cover and cooling in alb70-90N, sensible and latent heat fluxes from the surface to the atmosphere over the area 60°-90°N decrease by 0.03 PW and 0.07 ± 0.01 PW relative to the $4xCO_2$ simulation, respectively. Because of surface cooling, upward longwave radiation decreases by 0.28 ± 0.02 PW while downward longwave radiation decreases by 0.25 ± 0.02 PW, leading to a reduction in net longwave radiation from the surface of 0.04 ± 0.01 PW. (Decomposition of net surface flux into shortwave, longwave, latent and sensible heat fluxes is given in Supplementary Table 5). Thus in alb70-90N relative to $4xCO_2$, about 33% of the net shortwave energy loss at the surface is compensated by a reduction in latent heat fluxes, ~19% by a decrease in net longwave radiation from the surface and ~14% by a reduction in sensible heat fluxes. Resulting net surface energy loss of 0.07 ± 0.01 PW is thus only ~33% of the net surface shortwave energy loss. Partial compensation of net shortwave flux changes at the surface and the resulting net surface energy loss are illustrated in Supplementary Fig. 8a (for all of the simulations with imposed albedo modifications).

b) High latitude top-of-atmosphere (TOA) energy budget decomposition

We use the symbol 'TOA' to refer to top of model atmosphere values used to calculate energy variables within the climate model, not the derived values used for diagnostic comparison with satellite observations (Neale et al. 2010). TOA net shortwave energy flux to space in alb70-90N relative to the $4xCO_2$ simulation (see Supplementary Table 6) increases by 0.20 ±0.01 PW (similar to the 0.21 ± 0.01 PW increase in net surface shortwave flux to the atmosphere). This change in net shortwave TOA flux originates solely from an increase in upward shortwave TOA flux by the same amount (0.20 ±0.01 PW). Net TOA longwave flux to space decreases by 0.05 ± 0.01 PW (similar to the decrease in surface net longwave flux to the atmosphere). This change in net TOA longwave flux is mainly due to a decrease in upward longwave flux of 0.04 ± 0.01 PW. Imposed surface albedo alterations in alb70-90N relative to the $4xCO_2$ simulation thus lead to 0.16 ± 0.01 PW additional energy loss at the top of the model over the area 60°-90°N.

Interestingly, in all simulations with imposed albedo modifications relative to the $4xCO_2$ simulation (with no albedo modifications), high latitude net shortwave flux changes are effectively the same at the surface and at the top-of-atmosphere (Supplementary Tables 5 and 6). This is however not the case when comparing the simulations with different CO_2 concentrations (e.g., alb70-90N and $1xCO_2$).

Net TOA energy loss over the area 60°-90°N is also an estimate of the increase in implied total heat transport across 60°N with net surface energy loss being an estimate of the increase in implied ocean heat transport across 60°N. Thus, in alb70-90N relative to $4xCO_2$, ~44% of the change in TOA energy flux over 60°-90°N (implied total heat transport across 60°N) is offset by a change in surface energy flux (implied ocean heat transport through 60°N) and ~ 56% is offset by a change in implied atmospheric heat transport through 60°N. Atmospheric heat transport changes are discussed shortly.

It has been conjectured that there is an adjustment mechanism that causes the top-of atmosphere reflected shortwave radiation to be nearly equal in both hemispheres, despite interhemispheric differences in surface albedo (Voigt et al. 2013). Our simulations do not support such findings. For example, in alb70-90N relative to 1xCO_2, northern hemisphere TOA upward shortwave flux decreases by 0.18 ± 0.01 PW, whereas the southern hemisphere TOA upward shortwave hemisphere flux change equals only 0.01 ± 0.02 PW.

c) Clear- and cloudy-sky flux changes

The role of clouds in modulating the surface energy budget over the area 60°-90°N can be highlighted by considering the fluxes over the cloud free (clear-sky) and cloud covered (cloudy-sky) areas. Any (all-sky) variable F can be expressed in terms of its clear-sky and cloudy-sky components, FC and FCL, using the following relation:

$$F = (1 - CLDFRC) \cdot FC + CLDFRC \cdot FCL, \quad \text{(S1)}$$

where *CLDFRC* is a total cloud fraction in a given cell.

In alb70-90N relative to 4xCO_2, over the area 60°-90°N, net shortwave clear-sky flux from the surface increases by 0.56 ± 0.01 PW (mainly due to an increase in upward shortwave clear-sky flux of 0.61 ± 0.01 PW). Net shortwave cloudy-sky flux from the surface increases by only 0.10 PW (a result of 0.32 ± 0.01 PW increase in upward shortwave flux and 0.22 ± 0.01 PW increase in downward shortwave flux). Net longwave clear-sky flux into the atmosphere decreases by 0.12 ± 0.01 PW while net cloudy-sky longwave flux decreases by 0.06 ± 0.01 PW.

At the model top, net shortwave clear-sky energy flux to space over the area 60°-90°N increases by 0.53 ± 0.01 PW (comparable to 0.56 ± 0.01 PW increase in clear-sky flux from the surface). TOA net shortwave full-sky energy flux to space increases by 0.09 ± 0.01 PW (similar to the 0.10 PW at the surface). Thus, both clear-sky and cloudy-sky net shortwave flux changes in alb70-90N relative to 4xCO_2 are effectively maintained at the top of the model. However, it is interesting to note that this is only the case for the net shortwave fluxes. Upward and downward shortwave flux anomalies at the surface are not maintained at the top of atmosphere, only their sum is. As a consequence, shortwave albedo changes (defined as a ratio of reflected to incident radiation) differ at the surface and model top. Attenuation of surface albedo changes is largest in case of all-sky fluxes, but it is also present when considering the clear-sky fluxes (Supplementary Table 2). For example, in 4xCO2 simulation, clear-sky TOA albedo value is ~92% of the clear-sky surface albedo value, while in alb70-90N, clear-sky TOA albedo value is ~85% of the surface albedo value. Change in clear-sky TOA albedo between alb70-90N and 4xCO2 becomes 65% of the corresponding change in clear-sky surface albedo.

d) Atmospheric heat transport across 60°N

Atmospheric heat transport (AHT) changes relative to the $1xCO_2$ simulation are plotted in Supplementary Fig. 9 a and b, accompanied by latent heat and dry static energy transport anomalies in panels 9c and 9d.

In $4xCO_2$ relative to the $1xCO_2$ simulation, overall atmospheric heat transport across 60°N does not change noticeably. However, there is a shift in partitioning between AHT components, leading to a decrease in dry static energy (DSE) transport and increase in latent heat (LH) transport. In simulations with imposed albedo modifications, this decrease in DSE transport relative to the $1xCO_2$ value is still present, but it is considerably smaller than in the $4xCO_2$ simulation. Latent heat transport changes across 60°N, on the other hand, are much smaller, and depending on the case act to either partially attenuate or strengthen the DSE transport changes. As a result, overall atmospheric heat transport across 60°N increases in all simulations with imposed albedo modifications (relative to the $4xCO_2$ simulation). For example, in alb70-90N relative to $4xCO_2$, LH transport increases by ~0.01PW and DSE transport increases by ~0.08 PW, leading to an atmospheric heat transport increase of 0.09±0.01 PW across 60°N. AHT, DSE and LH transport values are given in Supplementary Table 7.

e) Subsurface temperature responses

On the time scales considered in this study we find only modest impacts of imposed albedo changes and sea ice recovery on high latitude subsurface land temperatures. However, it is not excluded that more substantial impacts could develop when considering longer time periods.

Imposed albedo modifications show only a modest impact on Arctic permafrost: 33-44% of preindustrial permafrost area remains in simulations with ocean albedo alterations compared to 32% in the $4xCO_2$ control simulation (Supplementary Fig. 10).

f) Impact of ocean albedo alteration under lower CO_2 concentrations

We have preformed an analogue to the alb70-90 simulation, using the $1xCO_2$ as our background climate (alb70-90_1xco2). We find the ratios of recovered sea ice area to altered ocean albedo area to equal 80% in the simulation with albedo modifications imposed over 70°-90°N in the $1xCO_2$ climate, compared to 75% when the same modifications are imposed in the $4xCO_2$ climate. (Annual mean altered albedo area in alb70-90_1xco2 equals 1.27±0.02 million km^2, while the annual mean recovered sea ice area equals 1.01± 0.07 million km^2). As expected, the colder $1xCO_2$ climate allows for easier sea ice recovery in the presence of albedo changes, demonstrating the sensitivity of the impact of ocean albedo alterations on the background climate.

g) Spatial averaging

Over a region R at time t, for each two-dimensional variable F we define a regional weighted area sum $FSUM$ as:

$$FSUM_{R,t} = \sum_{(i,j)\in R} area_{i,j} F_{i,j,t} \quad \text{(S2)}$$

where i, j are the grid cells indices within the region R and $area_{i,j}$ is area of the corresponding gird cell.

Total area of region R is then:

$$area_R = \sum_{(i,j)\in R} area_{i,j}. \quad \text{(S3)}$$

Weighted area average of variable F over the region R, $F_{R,t}$, is derived as a ratio of $FSUM_{R,t}$ and the area of region R:

$$F_{R,t} = \frac{FSUM_{R,t}}{area_R} = \frac{\sum_{(i,j)\in R} area_{i,j} \cdot F_{i,j,t}}{\sum_{(i,j)\in R} area_{i,j}} \quad \text{(S4)}$$

Supplementary Figures:

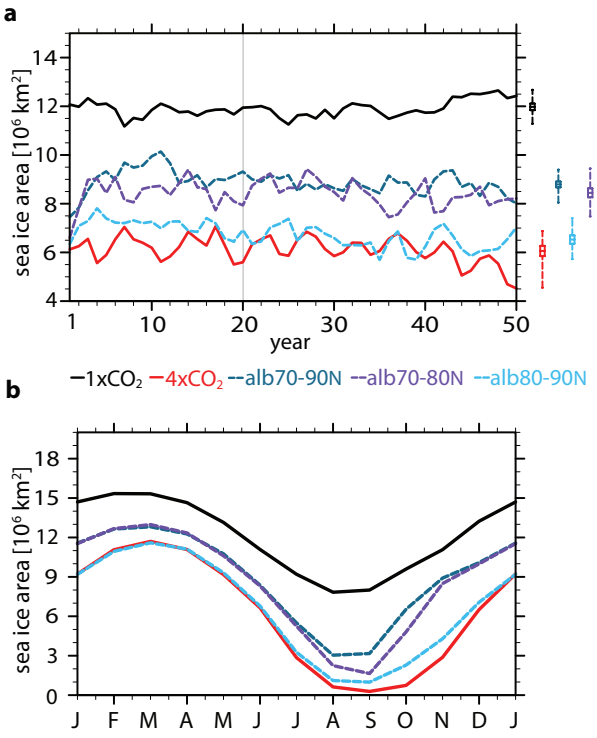

Supplementary Fig. 1: (a): Annual Arctic sea ice areas over the last 50 years of model integration. Boxes on the right show the mean with two standard errors while whiskers indicate min/max range (over the last 30 years). (b): Monthly mean Arctic sea ice areas (over the last 30 years of model integration). 1xCO_2 simulation – black solid line, 4xCO_2 simulation – red solid line, alb70-90N – dark blue dashed line, alb80-90N – light blue dashed line, alb70-80N – dark purple dashed line.

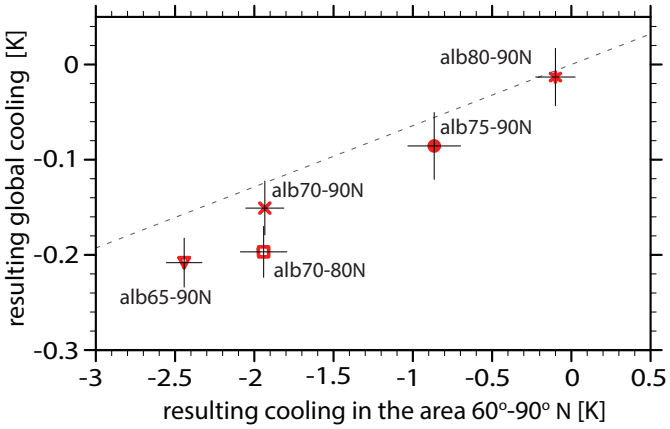

Supplementary Fig. 2: Global annual mean temperature anomalies [K] versus high latitude (60°-90°N) temperature anomalies (both relative to $4xCO_2$). The dashed line shows the ratio of high latitude to global cooling if there was no change in temperature outside the area 60°-90°N. The largest global and local temperature responses per unit area of imposed ocean albedo modifications are achieved in alb70-80N simulation, which also had the largest cooling effect outside of 60°-90° N.

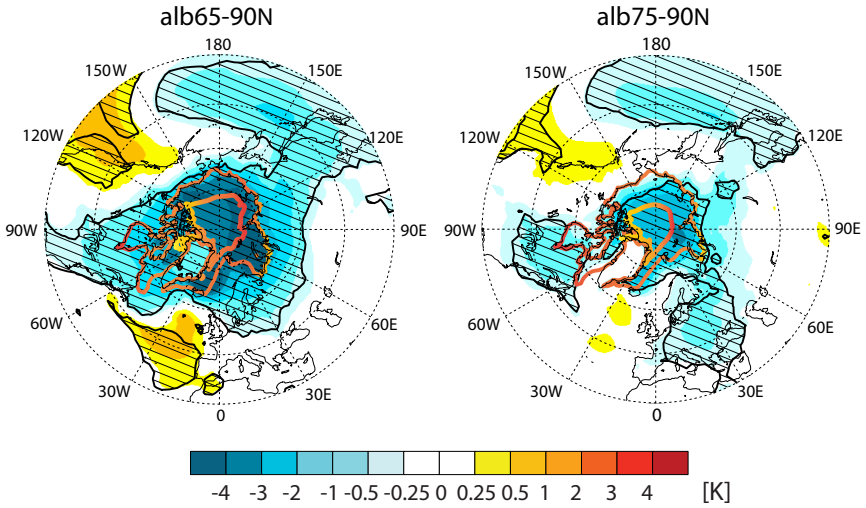

Supplementary Fig. 3: Annual surface air temperature anomalies [K] between 30°N and 90°N in alb6590N and alb7590N relative to the $4xCO_2$ simulation. Dashed areas indicate the anomalies that are statistically significant at the 95% confidence level. Both simulations show notable warming off the west coast of North America (in addition to the Arctic cooling). Thin and thick contour lines indicate the areas with annual mean sea ice fractions larger than 15% and 80%, respectively.

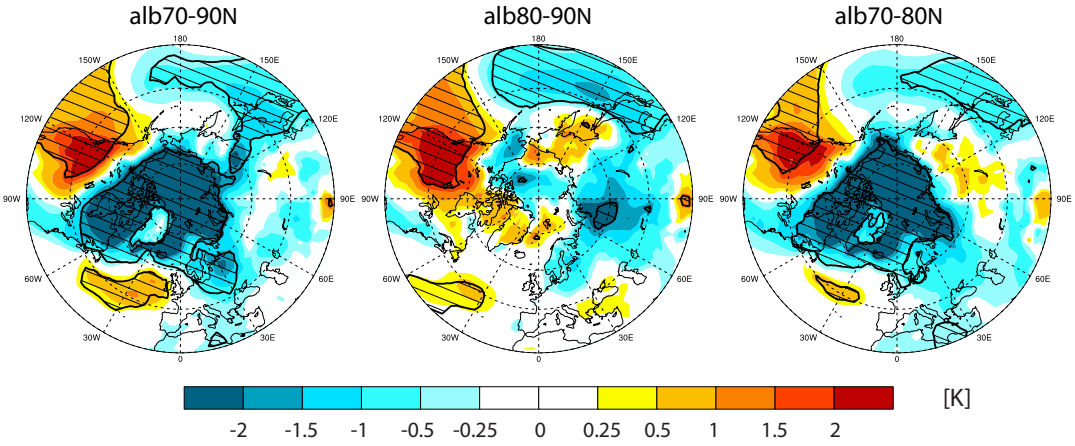

Supplementary Fig. 4: January surface air temperature anomalies [K] in modified ocean albedo simulations relative to the 4xCO_2 simulation. Dashed areas indicate the anomalies that are statistically significant at the 95% confidence level.

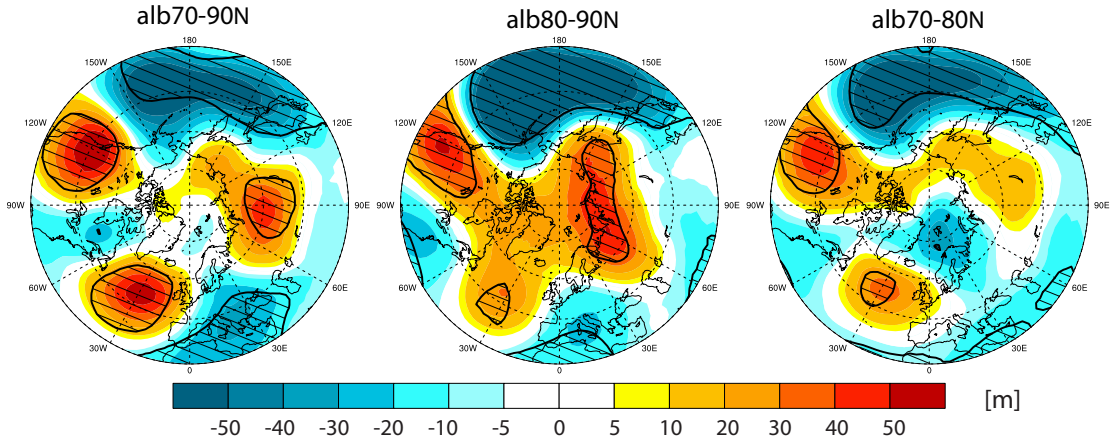

Supplementary Fig. 5: January 500hPa geopotential height anomalies in modified ocean albedo simulations relative to the 4xCO_2 simulation, units: [m]. Dashed areas indicate the anomalies that are statistically significant at the 90% confidence level.

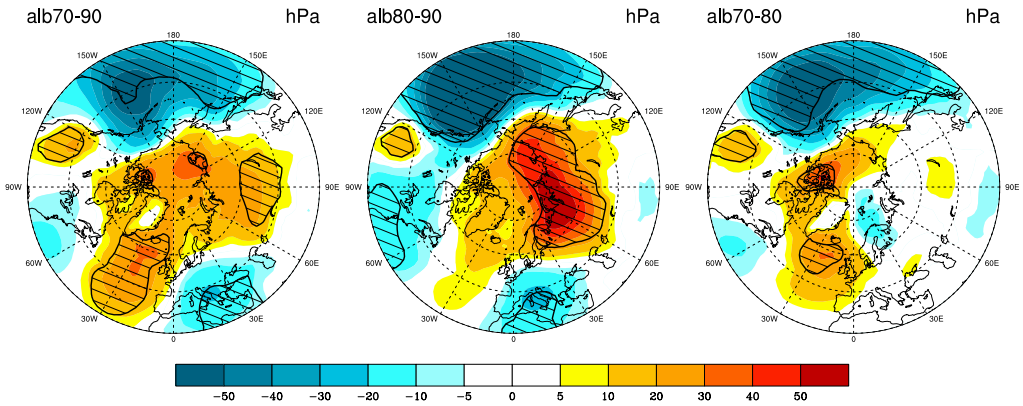

Supplementary Fig. 6: January surface pressure anomalies in modified ocean albedo simulations relative to the $4xCO_2$ simulation, units: [hPa]. Dashed areas indicate the anomalies that are statistically significant at the 90% confidence level.

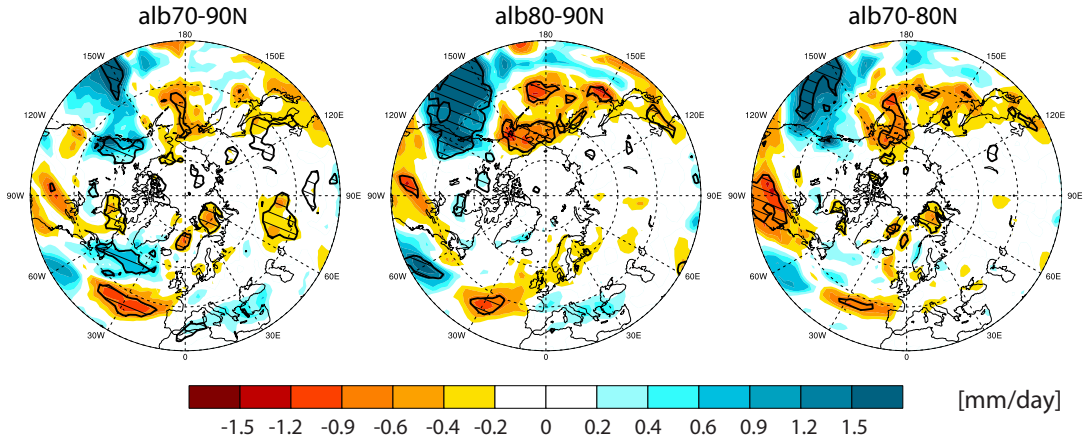

Supplementary Fig. 7: January precipitation anomalies [mm/day] in modified ocean albedo simulations relative to the $4xCO_2$ simulation. Dashed areas indicate the anomalies that are statistically significant at the 95% confidence level.

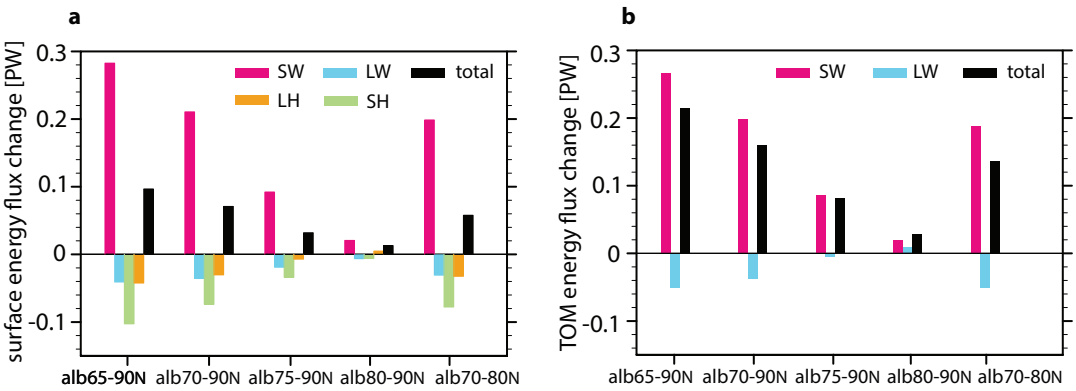

Supplementary Fig. 8: (a) Surface and (b) top-of-atmosphere (TOA) annual mean energy flux anomalies over the area 60°-90°N in simulations with imposed albedo alterations relative to the 4xCO_2 simulation. Positive anomaly means increase in the upward flux. Legend: SW - net shortwave flux, LW - net longwave flux, LH - latent heat flux, SH - sensible heat flux, total - sum of all surface/TOA fluxes. The heights of SW bars in panels a in b indicates similar change in shortwave net flux at the surface and model top.

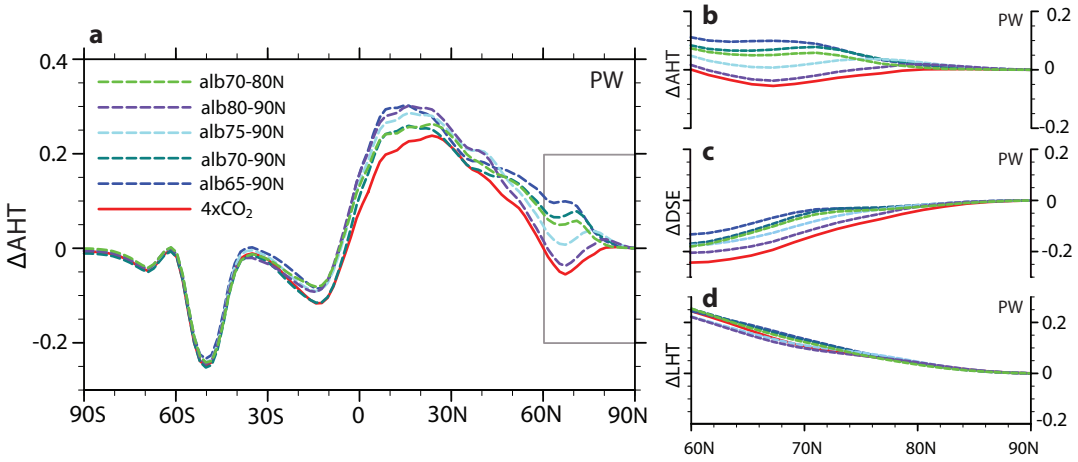

Supplementary Fig. S9: Atmospheric heat transport (AHT) anomalies [PW] relative to the 1xCO_2 simulation and its high latitude decomposition into dry static energy (DSE) and latent heat (LH) transport. AHT, DSE and LH transports across 60°N are summarized in Supplementary Table 7.

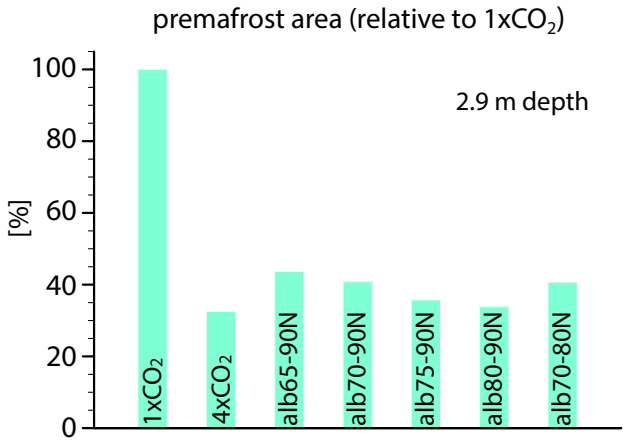

Supplementary Fig. 10: Remaining Northern hemispheric permafrost area relative to the $1xCO_2$ simulation [%]. Over the time scales considered in this study, imposed albedo modifications have lead to a small increase in permafrost area.

Supplementary Tables:

Supplementary Table 1: Annual mean altered albedo area, annual mean and September Arctic sea ice extents and annual mean surface air temperatures (60°-90°N and global) over the last 30 years of model integration (mean and one standard error).

	Annual mean altered albedo area [millions of km^2]	Annual mean Arctic sea ice area [millions of km^2]	September Arctic sea ice extent [millions of km^2]	60°-90°N annual mean surface air temperature [°C]	Global annual mean surface air temperature [°C]
1xCO_2	0	11.93±0.07	8.00±0.10	-12.19±0.12	13.77±0.02
4xCO_2	0	6.06±0.09	0.28±0.04	-2.95±0.11	18.24±0.03
alb65-90N	4.96±0.04	9.28±0.05	3.58±0.14	-5.39±0.08	18.03±0.02
alb70-90N	3.67±0.05	8.81±0.06	3.17±0.16	-4.88±0.09	18.08±0.02
alb75-90N	1.76±0.04	7.52±0.07	1.90±0.12	-3.81±0.11	18.15±0.02
alb80-90N	0.97±0.03	6.49±0.08	0.99±0.09	-3.05±0.11	18.22±0.02
alb70-80N	3.23±0.05	8.41±0.09	1.64±0.14	-4.89±0.12	18.04±0.03

Supplementary Table 2: Surface, top-of-atmosphere (TOA) and clear-sky top-of-atmosphere (TOA CS) albedo values averaged over the area 60°-90°N (± one standard error). All albedo values are calculated using the 30-year mean reflected and incident shortwave radiation.

	surf albedo 60°-90°N	CS surf albedo 60°-90°N	TOA albedo 60°-90°N	TOA CS albedo 60°-90°N
1xCO_2	0.520± 0.018	0.476± 0.014	0.540± 0.006	0.408±0.009
4xCO_2	0.375±0.018	0.338± 0.013	0.498±0.005	0.310±0.008
alb65-90N	0.522±0.011	0.499± 0.006	0.539±0.004	0.416±0.004
alb70-90N	0.490±0.012	0.463± 0.006	0.528±0.005	0.392±0.004
alb75-90N	0.431±0.014	0.399± 0.010	0.511±0.005	0.350±0.006
alb80-90N	0.392±0.018	0.357± 0.012	0.501±0.005	0.323±0.006
alb70-80N	0.480±0.013	0.449± 0.008	0.527±0.005	0.383±0.006

Supplementary Table 3: Surface and top-of-atmosphere (TOA) albedo values: global, northern and southern hemispheric means (± one standard error). All albedo values are calculated using the 30-year mean reflected and incident shortwave radiation.

	surface albedo global	surface albedo NH	surface albedo SH	TOA albedo global	TOA albedo NH	TOA albedo SH
1xCO_2	0.131±0.001	0.142±0.001	0.120±0.001	0.312±0.001	0.312±0.001	0.311±0.002
4xCO_2	0.115±0.001	0.125±0.001	0.106±0.001	0.302±0.001	0.303±0.001	0.301±0.001
alb65-90N	0.121±0.001	0.137±0.001	0.106±0.001	0.303±0.001	0.306±0.001	0.300±0.001
alb70-90N	0.120±0.001	0.134±0.001	0.106±0.001	0.303±0.001	0.305±0.001	0.301±0.001
alb75-90N	0.118±0.001	0.129±0.001	0.106±0.001	0.302±0.001	0.304±0.001	0.301±0.001
alb80-90N	0.116±0.001	0.126±0.001	0.106±0.001	0.302±0.001	0.303±0.001	0.301±0.001
alb70-80N	0.120±0.001	0.133±0.001	0.106±0.001	0.303±0.001	0.305±0.001	0.301±0.001

Supplementary Table 4: Annual mean top-of-atmosphere (TOA) and surface flux area-weighted sums. All fluxes are positive down. Values shown as mean ± one standard error.

	TOA net 60°-90°N area-weighted sum [PW]	surf net 60°-90°N area-weighted sum [PW]	TOA net NH area-weighted sum [PW]	surf net NH area-weighted sum [PW]	TOA net SH area-weighted sum [PW]	surf net SH area-weighted sum [PW]
1xCO_2	-3.31±0.00	-0.48±0.01	-0.52±0.02	-0.54±0.02	0.46±0.02	0.50±0.02
4xCO_2	-3.21±0.01	-0.40±0.01	-0.29±0.02	-0.22±0.02	0.96±0.02	0.90±0.02
alb65-90N	-3.43±0.01	-0.50±0.01	-0.52±0.02	-0.37±0.01	1.02±0.01	0.89±0.01
alb70-90N	-3.37±0.01	-0.47±0.01	-0.44±0.02	-0.34±0.02	0.99±0.01	0.89±0.01
alb75-90N	-3.29±0.01	-0.43±0.01	-0.38±0.02	-0.25±0.01	1.00±0.01	0.88±0.01
alb80-90N	-3.24±0.01	-0.41±0.01	-0.37±0.02	-0.22±0.01	1.01±0.02	0.87±0.02
alb70-80N	-3.35±0.01	-0.46±0.01	-0.43±0.02	-0.31±0.01	1.03±0.02	0.92±0.02

Supplementary Table 5: Decomposition of net surface flux over the area 60°-90°N into shortwave and longwave components. Values given as annual mean area-weighted sums (mean ± one standard error).

	net shortwave flux [PW] (*positive down*)	downward shortwave flux [PW]	upward shortwave flux [PW]	net longwave flux [PW] (*positive up*)	downward longwave flux [PW]	upward longwave flux [PW]	latent heat flux [PW] * (*positive up*)	sensible heat flux [PW] (*positive up*)
1xCO_2	1.55±0.01	3.24±0.01	1.68±0.01	1.32	7.49±0.02	8.81±0.02	0.53	0.18
4xCO_2	1.77±0.01	2.84±0.01	1.06±0.01	1.23±0.01	8.84±0.02	10.06±0.02	0.68	0.26
alb65-90N	1.49	3.11±0.01	1.62±0.01	1.19	8.52±0.01	9.71±0.01	0.58	0.22
alb70-90N	1.56±0.01	3.06±0.01	1.50±0.01	1.19	8.59±0.01	9.79±0.01	0.61	0.23
alb75-90N	1.68±0.01	2.95±0.01	1.27±0.01	1.21	8.73±0.02	9.94±0.02	0.65	0.25
alb80-90N	1.75±0.01	2.88±0.01	1.13±0.01	1.22	8.83±0.02	10.05±0.02	0.67	0.27
alb70-80N	1.57±0.01	3.02±0.01	1.45	1.20	8.58±0.02	9.78±0.02	0.60	0.23

* Model output latent heat flux (LHFLX) was corrected to account for latent heat of sublimation of snow (see Kay et al. 2013).

Supplementary Table 6: Shortwave and longwave TOA flux components over the area 60°-90°N (annual mean area-weighted sums, mean ± one standard error).

	net shortwave flux [PW] (*positive down*)	upward shortwave flux [PW]	net longwave flux [PW] (*positive up*)	upward longwave flux [PW]
1xCO_2	3.00±0.01	3.53±0.01	6.31±0.01	6.35±0.01
4xCO_2	3.28±0.01	3.25±0.01	6.49±0.01	6.53±0.01
alb65-90N	3.01	3.52	6.44±0.01	6.48±0.01
alb70-90N	3.08±0.01	3.45±0.01	6.45±0.01	6.49±0.01
alb75-90N	3.19±0.01	3.34±0.01	6.49±0.01	6.53±0.01
alb80-90N	3.26±0.01	3.27±0.01	6.50±0.01	6.54±0.01
alb70-80N	3.09±0.01	3.44±0.01	6.44±0.01	6.48±0.01

Supplementary Table 7: Annual mean atmospheric heat transport (AHT) across 60° and its components: latent heat (LH) and dry static energy (DSE) transports (mean ± one standard error).

	AHT [PW]	LH transport [PW]	DSE transport [PW]
1xCO_2	2.83±0.01	0.79±0.01	2.04±0.01
4xCO_2	2.81±0.01	1.01±0.01	1.80±0.01
alb65-90N	2.93±0.01	1.02±0.01	1.91±0.01
alb70-90N	2.90±0.01	1.02±0.01	1.88±0.01
alb75-90N	2.86±0.01	0.99±0.01	1.87±0.01
alb80-90N	2.83±0.01	0.99±0.01	1.84±0.02
alb70-80N	2.89±0.01	1.02±0.01	1.87±0.01

Supplementary Table 8: Dependence of the sea ice and surface temperature response on the strength of ocean albedo alteration. Experiments alb70-90Nval08 and alb70-90Nval07 are identical to the alb70-90N except that the albedo values are uniformly set to 0.8 and 0.7. Columns the same as in Table 1.

	Annual mean altered albedo area [millions of km^2]	Annual mean Arctic sea ice area [millions of km^2]	September Arctic sea ice extent [millions of km^2]	60°-90°N annual mean surface air temperature [°C]	Global annual mean surface air temperature [°C]
alb70-90N	3.67±0.05	8.81±0.06	3.17±0.16	-4.88±0.09	18.08±0.02
alb70-90Nval08	4.07±0.05	8.32±0.06	2.33±0.11	-4.58±0.08	18.11±0.02
alb70-90Nval07	4.13±0.06	8.30±0.08	2.21±0.14	-4.64±0.11	18.14±0.02

References:

Voigt, A., Stevens, B., Bader, J. & Mauritsen, T. Compensation of Hemispheric Albedo Asymmetries by Shifts of the ITCZ and Tropical Clouds. *J. Clim.* **27,** 1029–1045 (2014).

Neale, R. B. *et al. Description of the NCAR Community Atmosphere Model (CAM 4.0).* (2010).

Kay, J.E., Holland, M.M., Bitz, C.M., Blanchard-Wrigglesworth, E., Gettelman, A., Conley, A., Bailey, D. The Influence of Local Feedbacks and Northward Heat Transport on the Equilibrium Arctic Climate Response to Increased Greenhouse Gas Forcing. *J. Clim.* 25, 5433–5450 (2012). doi:10.1175/JCLI-D-11-00622.1